An Experimental Study of Space and Time-Resolved Structures of Turbulent Diffusion Flame*

Tamio IDA** and Kazutomo OHTAKE***

The authors discuss in detail the various heat transportation mechanisms existing in turbulent diffusion flames by use of spectral analyses. Space and time-resolved structures of turbulent diffusion flames were analyzed by two-point laser Rayleigh spectroscopy (LRS) which did not directly interfere with the combustion media during measurement. The turbulent diffusion flame structures were divided into 4 regions based on the characteristics of their spectral analysis of time-dependent temperature signals. In order to discuss the macroscopic heat transportation mechanism, the coherent function from cross and power spectral functions at Region I ~IV was analyzed. From these analyses, the following diffusion characteristics at each region were revealed. Region I : three-dimensional diffusion mechanism (x-, r-, z-axes), Region II : one-dimensional diffusion mechanism (z-axis), Region III : two-dimensional diffusion mechanism (x-, z-axes), Region IV : no specific diffusion mechanism.

Key Words: Turbulent Diffusion Flame Structure, Laser Rayleigh Spectroscopy, Two-Point Measurement, Thermal Mechanism, Coherent Function

1. Introduction

Space- and time-resolved fundamental information, such as velocity, temperature and concentrations of chemical species, is quite essential for the detailed study of mixing, reaction and heat transportation mechanisms in turbulent diffusion flames. The turbulent diffusion flame changes its characteristics on working conditions such as burner sizes, types of fuel and oxidant, their velocities, etc. The flame structures vary widely from those maintaining the characteristics of laminar flames to those of highly turbulent non-premixed ones.

Recently, new laser spectroscopy techniques have been adopted to analyze the planar images of scalar quantities in the reacting flows by using a laser sheet as an incident light source[1]-[7]. Such spatial information cannot yet explain the heat-transfer mechanisms occurring in the mixing process without additional information. Various methods such as fluorescence and Mie scattering have been used to measure the species concentrations and instantaneous shapes of flame and/or fuel flow. With planar fluorescence spectroscopy it is scare to obtain qualitative information covering the entire observation area since it is rather hard to excite all the target molecules up to the saturated condition. On the other hand, the Mie scattering method is the easiest technique to obtain the plane images, however, the difficulty in uniform introduction of fine particles into the flow remains as a problem. An LRS can measure the time-resolved gas temperature in the reaction flow if the bulk scattering cross sections of air, fuel and combustion gas does not change so much.

Dibble et al.[8] and Schoenung et al.[9] studied non-premixed turbulent flames by LRS and discussed the difference in flame structure between turbulent non-premixed and premixed flames. They obtained pdf (probability density function), power spectral density

* Received 27th May, 1996. Japanese original: Trans. Jpn. Soc. Mech. Eng., Vol. 61, No. 584, B (1995), pp. 1547-1553 (Received 14th July, 1994)

** Department of Mechanical Engineering, Kumano Technical College, 2800 Arima-cho, Kumano, Mie 519-43, Japan

*** Department of Ecological Engineering, Toyohashi University of Technology, 1-1 Tempaku-cho, Toyohashi, Aichi 441, Japan

function and other statistical values. The upper limit for frequency response of 5 kHz in their diagnostics still remains the blind part for the phenomena occurring in the higher frequency region. Namazian presented the three dimensional visualizations of flame sheet in premixed flame measured by two points LRS method[10].

In our previous studies, the turbulent diffusion flame structures were studied by time-resolved various laser probes[11]-[14]. The turbulent time scale therein was obtained from the temperature fluctuations by one-point LRS. The flame could be divided into four regions based on the characteristics of time scale. A two color forward scattering 2 W Ar ion laser-soured LDV system at 488 and 514.5 nm was utilized together with LRS system simultaneously to decide the axial and radial velocities. The turbulent fluxes of momentum and heat ($\overline{u'v'}$ and $\overline{u'T'}$, $\overline{v'T'}$) at one point were obtained. The turbulent Reynolds stress $\overline{u'v'}$ is proportional to the gradient of time mean axial velocity ($\partial\bar{U}/\partial r$) in all regions. On the other hand, turbulent heat flux $\overline{v'T'}$ shows proportionality to the gradient of time mean temperature ($\partial\bar{T}/\partial r$) at almost all the places of flame except the flame region (Region II). This means that the simple turbulent model $\overline{v'T'}\propto(\partial\bar{T}/\partial r)$ may not be applied at the combustion zone especially near the maximum time mean temperature. The time-dependent phenomena have often been masked by the statistical analyses, and spatial structures of turbulent diffusion flames are not yet fully understood. Schlieren and laser sheet Mie scattering photographs were taken simultaneously by a high speed video camera to correlate the signal measured by the above laser probe system with the phenomena occurring in the measuring field. The Rayleigh scattering signals were compared with high speed Schlieren and laser sheet Mie scattering photographs and the correspondence of characteristics of the signals to the phenomena happening in the flame was discussed. From this method the spatial and time resolved structures of turbulent diffusion flame became clearer.

This study discusses in detail the macroscopic heat transportation mechanisms of time dependent spatial and time-resolved turbulent diffusion flame by two-point LRS measurement. Space and time resolved structures of turbulent diffusion flame were obtained by two-point LRS which had no direct interference with the combustion media during measurement. Typical macroscopic structures were found to corresponding the mixing and reacting mechanisms in these regions.

Table 1 Experimental conditions

Exit conditions : D =4mm, Re = 5,000, x/D = 20
Mixed fuel : 62.2% H_2 + 37.8% CH_4
Measured points : r = 0 ~ 20 mm
$T_1(x+\Delta x, r+\Delta r, \Delta z) = T_1(80, r, 0)$
$T_2(x+\Delta x, r+\Delta r, \Delta z)$ =
$T_2(80+\Delta x, r, 0)$: Δx = 1.2 , 2.1 , 4.4 (mm)
$T_2(80, r+\Delta r, 0)$: Δr = 1.0 , 2.9 , 4.6 (mm)
$T_2(80, r, \Delta z)$: Δz = 1.0 , 2.9 , 4.6 (mm)

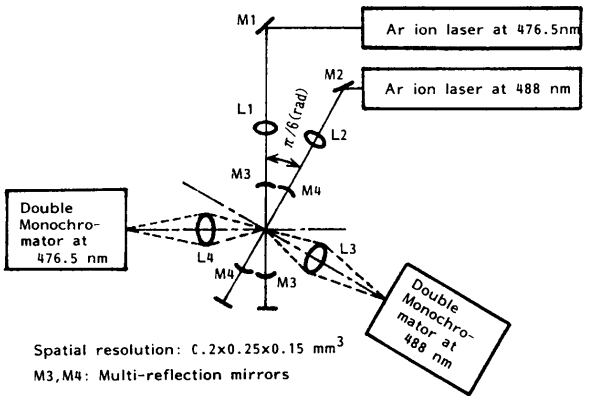

Fig. 1 Experimental apparatus

2. Experimental Apparatus

Figure 1 shows a layout of experimental apparatus. The LRS method by the incident wave-lengths of 476.5 and 488 nm emitted from two argon ion lasers was adopted to measure the two-point spatial correlation of time-resolved temperature. The experimental apparatus comprised Ar ion laser and spherical multi-reflection mirrors, double monochromator, photo multiplier. Especially, a pair of spherical multi-reflection mirrors reflected the laser light about ten times to intensify the incident light power at the focused point. These light beams were trimmed to prevent interference and let them cross at $\pi/6$ rad on construction.

Table 1 shows experimental conditions. The mixed gaseous fuel of 62.2% H_2+37.8% CH_4 was fed to the burner, inner diameter of which was 4 mm, and surrounded by the coaxial air duct of 64 mm I. D. The reason why this mixed fuel was selected was that its Rayleigh cross section did not change more than 5% from that of air, fuel and combustion gas before, during and after combustion. The detecting system can follow the phenomena up to 10 kHz, and be considered as having the satisfactory performance to measure the turbulent diffusion flame structures. All the signals obtained were recorded by a PCM recorder and processed by a computer and an FFT analyzer.

The distance of the two focusing points is varied along the Cartesian coordinates (x-, r-, z-axes).

3. Results and Discussions

3.1 Fundamental flame structure

In order to obtain the statistical values of temperature measured by LRS system, 100 000 data values recorded by the PCM recorder with sampling frequency of 50 kHz were analyzed. Coaxial turbulent diffusion flame at moderate Reynolds numbers, which maintain typical diffusion flame structures, were formed on laboratory-scale burners.

Time mean temperature distribution and time scale distribution of temperature fluctuation in turbulent diffusion flame at $D=4$ mm, $Re=5\,000$, $x/D=20$ are shown in Fig. 2. In the previous studies, it is found that the flame can be divided into four characteristic regions described below based on their spectral analysis and the distributions of macroscale of time-dependent temperature fluctuations. The $-5/3$ power law holds in the fuel jet and combustion regions. In the air entrainment regions, however, the $-5/3$ and -1 power laws coexist, and this shows that both turbulent and molecular heat transportations become important. Region I : This region exists in the central region of flame where the homogeneous temperature fluctuation is produced by heat transportation based on the turbulent diffusion of the heat and combustion products produced in the combustion regions. Region II : This region exists just outside Region I. The Maximum time mean temperature appears, and the time scale of temperature fluctuation steeply increases. This show that the entrained air penetrates into this region and combustion takes place at the interface between fuel and air. Region III : This region shows the characteristic that time mean temperature steeply decreases while time scale of temperature fluctuation is kept almost constant. This region could be defined as the region where the outside air flow is entrained into the flame region by the large scale eddies produced by the buoyancy of hot combustion gas. Region IV : The air flow region is surrounding outside Region III.

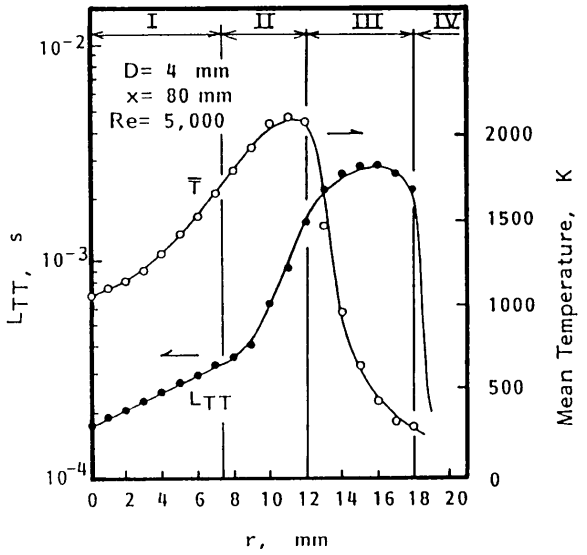

Fig. 2 Radial distribution of time temperature and time scale by time dependent temperature

Especially, in order to discuss the macroscopic heat transportation mechanism, coherent functions of three directions by cross and power spectral function in Region I ~IV were analyzed.

3.2 Space and time-resolved flame structures

The authors discuss in detail typical analyzed results and its statistical characteristics of space and time-resolved flame structure to the three directions. Especially, this could be grasped of time dependent spatial turbulent diffusion flame structures in region III remarkably occurred hydrodynamic mixing process by buoyancy force. Figures 3(a)-(c) show time-dependent temperature and its space-time cross correlation functions during 40 ms of simultaneous two points measurement at $x/D=20$, $\Delta x=1.2$ mm. Figure 4 shows the flame structure in Region III.

Figure 3(a) shows that correspond to lateral-axis is up-stream temperature, vertical-axis is down-stream temperature. Region I shows that weakly cross correlation like quasi-auto-correlation formations corresponds to weakly homogeneous turbulence. Region II negative correlation appears, but correlation is not remarkable. A temperature level increases, and its fluctuation is large. On the contrary, Region III shows a clear correlation and strong cross correlation. The arrow shows the direction of correlation movement as the function of time. This region shows the slop of $\pi/4$ rad in the correlation of time-dependent temperature signal. And also the correlation rotates clockwise and the track forms an elliptic shape. This slope suggests that the homogeneous heat transfer in the main flow direction dominates in this region. And also the negative time mean temperature gradient exists. Tables 2 and 3 show the results of quantitative analysis by the four quadrant method applied to evaluate the rotational direction and its heat transportation mechanisms. Figure 4 shows the schematic model of the movement of simplified flame structure in this region. The probability of correlation existing in first quadrant ($T_u'>0$, $T_d'>0$) is about 35%, while that in 3rd quadrant ($T_u'<0$, $T_d'<0$) about 40%, most of the probability exists in these two quadrants. About 70% of rotation occur to opposite clockwise direction. The 1st quadrant corresponds to the condition that both probing points exist in combustion gas. On the

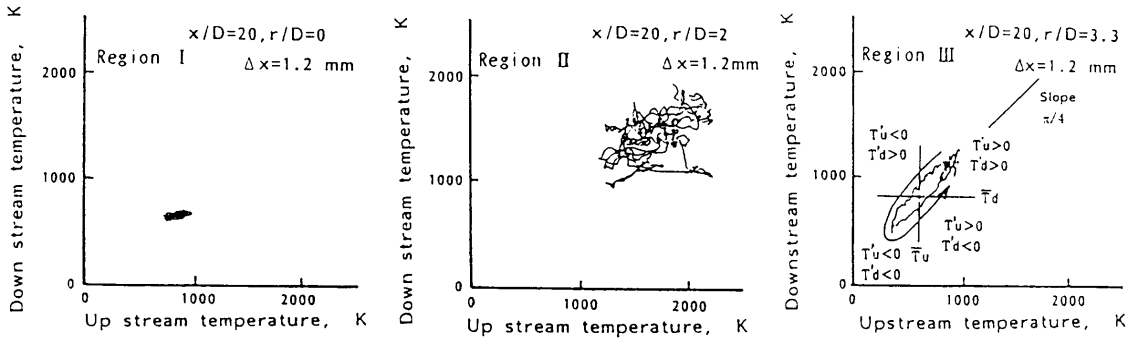

Fig. 3(a) Correlation of time dependent temperature

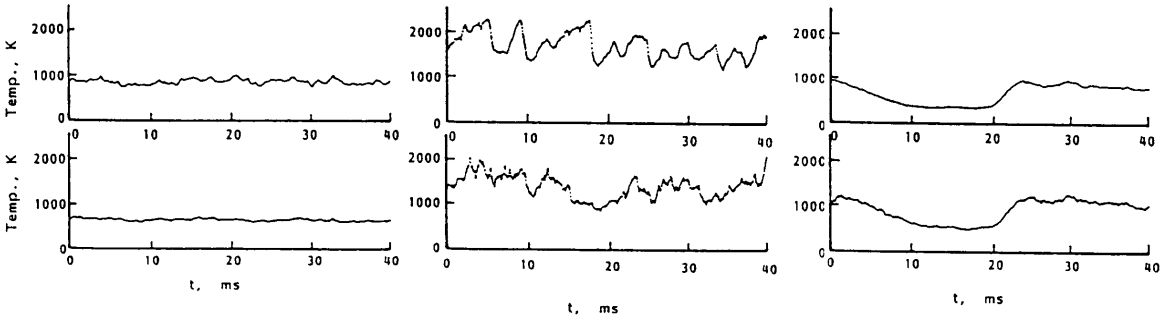

Fig. 3(b) Time dependent temperature signals

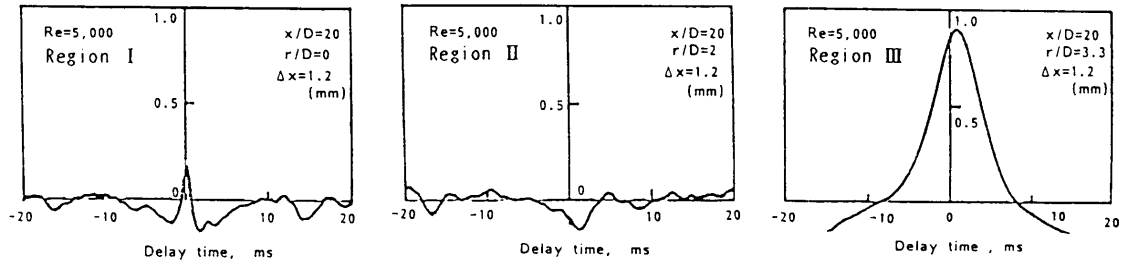

Fig. 3(c) Spatial-time cross correlation functions

Table 2 Probability of each region by 4 quadrant method

r(mm)	R①	R②	R③	R④	Region
0	31.20	19.60	31.12	18.08	I
2	29.36	20.00	33.84	16.80	
4	29.86	18.58	36.94	14.62	
6	36.08	14.24	32.44	17.24	
8	32.14	16.88	34.66	16.32	II
10	26.90	27.66	17.78	27.66	
12	27.10	24.62	17.22	31.06	
14	48.00	8.40	39.98	3.62	III
16	40.46	6.06	49.48	4.00	
18	19.46	10.36	50.06	20.12	
20	30.42	18.92	24.36	26.30	

Table 3 Rotational direction probability by 4 quadrant method

r(mm)	R①R②R③R④R①	R①R④R③R②R①	Region
0	49.50	50.50	I
2	44.60	55.40	
4	46.00	54.00	
6	35.50	64.50	
8	62.50	37.50	II
10	80.50	19.50	
12	41.50	58.50	
14	60.00	40.00	III
16	80.50	19.50	
18	66.00	34.00	
20	70.00	30.00	

contrary, the 3rd quadrant means the both points touch air at the same time. The results are summarized in Tables 2 and 3. These results could tell that the temperature difference between both points show the moving direction of burning zone, size of an elliptic region depends on the moving direction of burning zone or air region. However, heat transportation mechanisms occur to clockwise direction in spite of small probability about 30%. This says that the time mean heat transportation could not show the real measure of the phenomena or the time-resolved flame structure. From this method the multi-layered combustion zone in Region III could be observe as moving

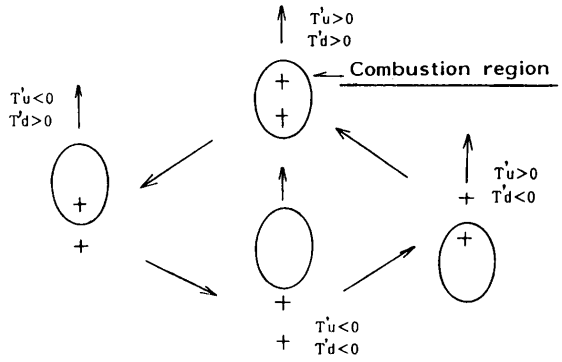

Fig. 4 Simply flame structure in Region III by 4 quadrant method

upward with rotation. Combining these results with the characteristics of coherent function. This region can be characterized as possessing the two-dimensional structure in its instantaneous flame structure. The same tendency could be observed when the distance between two points is changed. We understand that the whole structure of flame region in Region III moves upward (x-direction) by buoyancy with rotating fine structure. This characteristic could be understood more by comparison with the series of Schlieren photography reported in previous papers[1),(14)].

3.3 Flame structure based on heat transportation mechanism determined by coherent functions

In this section the heat transportation mechanism is discussed by coherent functions with spectral analysis on the frequency plane. Coherent function can be written as:

$$\mathrm{coh}^2(f)=\frac{|S_{12}(f)|}{S_{11}(f)S_{22}(f)} \qquad (1)$$

where $S_{12}(f)$ is defined by cross correlation function between points 1 (upstream measuring point) and 2 (downstream measuring point), $S_{11}(f)$, $S_{22}(f)$ express each power spectral function at the one point.

The coherent functions obtained in case of two points are conditional sampling of heat transportation corresponds to two points distance on the frequency plane. Therefore, we could demonstrate the spatial change of heat transportation mechanism with changing distance between two points. Figures 5(a)-(c) show the coherent function at each region corresponding to that in Table 1.

Firstly, we discuss heat transportation mechanisms in region I. In Fig. 5(a), coherent functions in three direction scarcely change and the heat transportation occurs around the heat transportation decreased gradually with increasing Δx with keeping its distribution profile at central frequency of 500 Hz. It spreads homogeneously in the space. Heat transportation decreases steeply with increasing Δr and Δz.

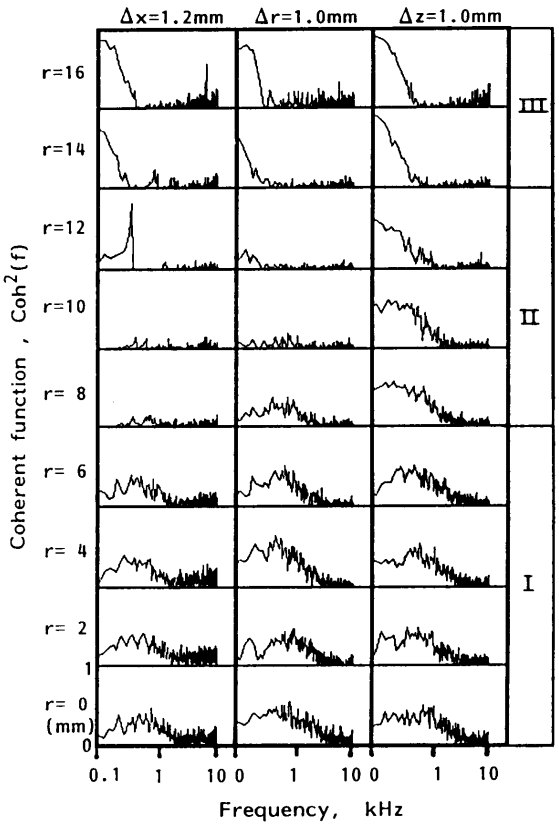

Fig. 5(a) Spatial distribution of coherent functions ($\Delta x=1.2$ mm, $\Delta r=1.0$ mm, $\Delta z=1.0$ mm)

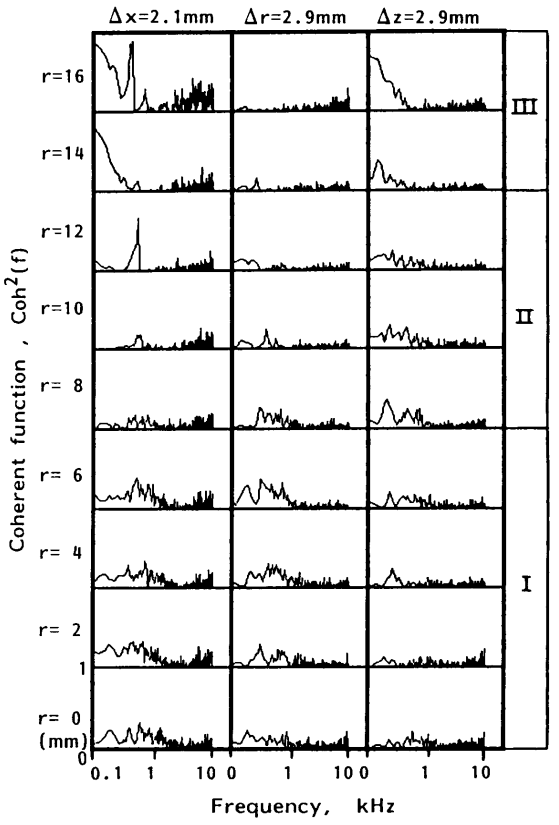

Fig. 5(b) Spatial distribution of coherent functions ($\Delta x=2.1$ mm, $\Delta r=2.9$ mm, $\Delta z=2.9$ mm)

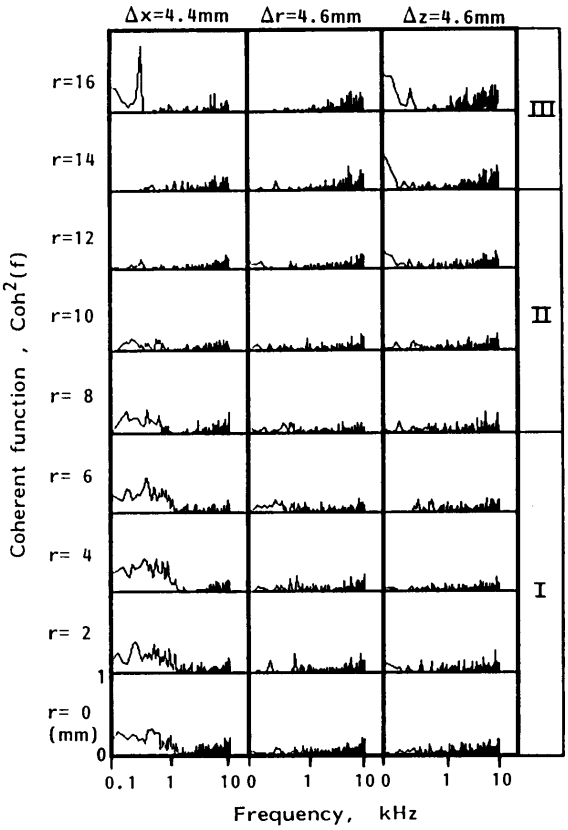

Fig. 5(c) Spatial distribution of coherent functions (Δx=4.4 mm, Δr=4.6 mm, Δz=4.6 mm)

This shows that in Region I monosized high temperature element eddy of about 1.5 mm distributes homogeneously, which is produced in Region II and transported into Region I by the entrainment flow with moving as spatial three dimensional.

In Region II heat transportation could not be found out except Δz=1.0 mm, the coherent strength of which is estimated as about 0.8 and central frequency of 200 Hz. Heat transportation can be classified as one dimensional structure. This region corresponds to combustion region existing at time mean maximum temperature by one-point measurement (LRS) as reported in previous study[11)-13)]. Turbulence is suppressed by the increase of kinematics viscosity with increasing flame temperature. An axial velocity of fuel flow is remarkably decreased because of the radial expansion of fuel stream. Complicated structure of layered burning zone consisting of fuel/air/combustion gas is rapidly transported downstream and heat transportation into x and r direction is limited. From these phenomenological views the geometrical size of fine structure in the combustion zone might be smaller than 1 mm, so that the coherent function in this region could not be detected.

Region III is the region where heat transportation occurs by periodic gas movement by buoyancy force which is caused by the periodically spaced high temperature combustion region. A coherent function in Region III describes a molecular heat transportation which is expressed by -1 power law of power spectral function in frequency zone appears at the frequency higher than 5 kHz. Macroscopic heat trans portation caused by the gas movement by buoyancy force appears at the frequencies lower than 200 Hz. The heat transportation mechanism to r direction hardly occurs because of the strong axial gas movement caused by buoyancy force. This characteristic remains in the combustion region at any distance between two points. As a result turbulent heat transportation occurs only in x and z direction in almost similar distributions.

Finally, we discuss heat transportation mechanism in radial direction. Coherent function in radial direction does not change so much in every region at any distance between the two points. Strong heat transportation signals appear at Δr=1.0 mm in every region, and steeply decrease with increasing the distance, but disappear at Δr>2.9 mm in every region. Heat transportation in z region appears at Δz=1 mm (Fig. 5(a)), but disappears at larger Δr at any radial position (Fig. 5(b),(c)). Region IV corresponds to the surrounding air flow region, and no turbulent heat transportation could be detected. From these analyses, the following heat transportation characteristics at each region have been concluded. Region I : three-dimensional diffusion (x-, r-, z-axes), Region II : one-dimensional diffusion (z-axis), Region III : two-dimensional diffusion (x-, z-axes), Region IV : no diffusion exists.

4. Conclusions

From the analyses based on coherent function, the following diffusion characteristics at each region were elucidated.

1) In Region III the ordered coherent turbulent flame structure caused by the buoyancy apparently exists, which is clearly understood by the four quadrant method.

2) It was shown that the heat transfer mechanism differs in four regions by the characteristic movement of bulk flow and flame structure in each region: Region I - Three dimensional diffusion (x-, r-, z-axes) dominates, Region II - One dimensional diffusion (z-axis), Region III - Two dimensional diffusion (x-, z-axes) does, respectively, Region IV - No apparent turbulent heat transportation exists.

3) It was pointed out that the time scale obtained by the one point LRS measurement corresponds to the macroscopic scale resulting from the layered structures in combustion zone, while the coherent function

distribution expresses the turbulent heat transportation mechanism corresponds to at the scale between the two points.

Acknowledgment

The partial funding from the Ministry of Education, Science and Culture under Contract Number 02209102 is acknowledged.

References

(1) Ohtake, K., et al., Trans. Jpn. Soc. Mech. Eng., (in Japanese), Vol. 57, No. 535, B (1991), p. 1135.
(2) Namazian, M. and Kelly, J.T., The 22nd Symposium (Int.) on Combustion, (1988), p. 627, The Combustion Institute.
(3) Chen, L.-D. and Roquemore, W.M., Comb. and Flame Vol. 66 (1986), p. 81.
(4) Mizutani, Y., et al., Trans. Jpn. Soc. Mech. Eng. (in Japanese), Vol. 54, No. 504, B (1988), p. 2219.
(5) Hanson, R.K., The 21st Symposium (Int.) on Combustion, (1986), p. 1677, The Combustion Institute.
(6) Long, M.B. and Yip, B., The 22nd Symposium (Int.) on Combustion, (1988), p. 701, The Combustion Institute.
(7) Long, M.B., Conference on Mechanism of Non-Uniform Combustion, (1990), p. 31.
(8) Dibble, R.W. and Hollenbach, R.E., The 18th Symposium (International) on Combustion, (1981), p. 1489, The Combustion Institute.
(9) Schoenumg, S.M. and Hanson, R.K., The 19th Symposium (Int.) on Combustion, (1982), p. 449, The Combustion Institute.
(10) Namazian, M., et al., The 19th Symposium (Int.) on Combustion, (1982), p. 487.
(11) Ohtake, K., et al., Trans. Jpn. Soc. Mech. Eng., Vol. 52, No. 482, B (1986), p. 3571.
(12) Ida, T., Ohtake, K., Trans. Jpn. Soc. Mech. Eng., Vol. 56, No. 531, B (1990), p. 3514.
(13) Ida, T., et al., The Japanese Symposium on Combustion, (1989), p. 19.
(14) Ohtake, K. and Ida, T., 5th Int. Symp. on Application of Laser Techniques to Fluid Mechanics, 31. 2, 1990.